PERGAMON

International Journal of Multiphase Flow 27 (2001) 701–719

International Journal of Multiphase Flow

www.elsevier.com/locate/ijmulflow

Anomalous velocity fluctuations in particulate turbulent channel flow

Koji Fukagata [a,c,*], Said Zahrai [b,c], Shunsuke Kondo [a], Fritz H. Bark [c]

[a] *Department of Quantum Engineering and Systems Science, University of Tokyo, 7-3-1 Hongo, Bunkyo-ku, Tokyo 113-8656, Japan*

[b] *ABB Corporate Research, 721 78 Västerås, Sweden*

[c] *FaxénLaboratoriet, Kungl. Tekniska Högskolan, 100 44 Stockholm, Sweden*

Received 14 December 1999; received in revised form 7 August 2000

Dedicated to Dr. Gad Hetsroni on his 65th birthday.

Abstract

Gas-particle turbulent channel flow at $Re_\tau = 644$, loaded with copper particles at a mass flow ratio of 2%, is studied numerically by large eddy simulation (LES) coupled with Lagrangian particle tracking (LPT). Inter-particle collisions and correction of drag force in the vicinity of walls are accounted for. Focus is made on the influence of particle wall boundary conditions and their influence on the statistical structure of the flow. It is shown that accordance with experimental data can be improved if a mechanism which can suppress the direct re-entrainment of particles after the impact at the wall is present. Present result shows that inter-particle collisions may play an important role in the re-distribution of particle momentum among different components even at low mass loading conditions.

Keywords: Two-phase flow; Gas-particle flow; Turbulence; Lagrangian particle tracking; Large eddy simulation; Inter-particle collision; Bimodality

1. Introduction

Gas-particle turbulent flows often appear in industrial processes. Examples of such are pollution control processes, food processing and material processing. Although many theoretical

* Corresponding author. Present address: Department of Mechanical Engineering, University of Tokyo, 7-3-1 Hongo, Bunkyo-ku, Tokyo 113-8656, Japan.

E-mail address: fukagata@thtlab.t.u-tokyo.ac.jp (K. Fukagata).

0301-9322/01/$ - see front matter
PII: S0301-9322(00)00049-5

studies have been done on such flow, they are limited in rather simple geometries with homogeneous turbulence or simple shear turbulence. However, in the real world applications, the flow is always confined by solid walls. Moreover, in many cases deposition and entrainment at walls are playing an important role in the process. Therefore, for many industrial systems, detailed understanding of wall-bounded gas-particle flows is of primary interest.

When the particle loading is high, the structure of turbulence is modified by the presence of particles, as has been observed in various experiments since the pioneering work by Hetsroni and Sokolov (1971) who studied the suppression of turbulence by adding droplets in a turbulent jet. Such turbulence modulation occurs in wall-bounded flows, too, as studied by Zisselmar and Molerus (1979) and Maeda et al. (1980) to name a few. Results of these experiments concerning the turbulence modulation are reviewed in Hetsroni (1989) and Gore and Crowe (1989).

Experimental investigations, however, have not been able to provide complete set of data for understanding the dynamics of the process. Turbulence modulation is an extremely complex phenomena far beyond the limit of applicability of analytical methods. The studies of turbulence modulation phenomenon is also important in industrial applications in addition to its academic value, as it may largely increase or decrease the transport of heat and mass. Therefore further and more detailed investigation should be done based on a solid basis. The first step of such investigation of a complex wall-bounded gas-particle flow may be an accurate prediction of motion and statistics of particles in simpler cases such as a dilute flow. In that case, the number density of particles is sufficiently low such that the structure of turbulence is not largely modified. The knowledge on such a dilute case will be a large building block to achieve the final goal, namely to understand the influence of particles on the structure of fluid turbulence.

Due to the explosive development of computer capacities, simulations of wall-bounded dilute gas-particle turbulent flows have become possible using rather direct methods. An example is the Lagrangian particle tracking (LPT), in which the trajectories of individual particles are computed by integrating the equation of motion for a particle. The turbulent fluid flow is usually simulated using a direct numerical simulation (DNS) or a large eddy simulation (LES) in an Eulerian frame.

Wang and Squires (1996) performed LPT simulations coupled with LES (LPT–LES) of gas-particle turbulent channel flows at $Re_\tau = 180$ and $Re_\tau = 644$. A dynamic subgrid scale model was used for LES. Lycopodium, glass and copper particles of different diameters were used. While the influence of fluid flow to particle motion was accounted for, the inverse influence of the motion of particle to fluid flow was neglected by an assumption of having very dilute flow, i.e., one-way coupling. The computed statistics for the cases of $Re_\tau = 180$ were in excellent agreement with the simulation data by Rouson and Eaton (1994), who used DNS instead of LES. Fukagata et al. (1998b) also performed one-way coupling LPT–LES for the same cases. Excellent agreement was found with the LPT–LES data by Wang and Squires (1996). For the cases with $Re_\tau = 644$, Wang and Squires (1996) compared their results with the experimental data for the cases for mass loading, Z, of 2% by Kulick et al. (1994). Large discrepancies were observed. For the case of 70 μm particles, for instance, the simulation predicted much higher mean particle velocity and much weaker wall-normal velocity fluctuations in the whole channel. The bimodality in the velocity distribution near the wall observed in the experiment by Kulick et al. (1994) was not reproduced in their simulations, either.

Tanaka et al. (1997) performed LPT–LES taking into account the influence of the particle motion to fluid flow and the inter-particle collisions, i.e., four-way coupling. They focused on the

cases of higher mass loading, $Z \geqslant 20\%$, which corresponds to the cases reported in experimental investigations by Kulick et al. (1994). They found that the inter-particle collisions have a strong influence on the statistics. The predicted wall-normal root-mean-square (RMS) particle velocity fluctuations in the bulk region of the channel for the case of 70 μm copper particles at $Z = 20\%$ was about 75% of the experimental data. This is twice as large as the result of a simulation neglecting the inter-particle collisions.

Fukagata et al. (1999) revisited the case with 70 μm copper particles at the lowest mass loading, $Z = 2\%$, in the experiment of Kulick et al. (1994). They performed four-way coupling LPT–LES considering the increase of drag in the vicinity of the wall (Faxén, 1923; Brenner, 1961) and found that inter-particle collisions have strong influence on the statistics. It has been assumed before that the mass flow ratio, $Z = 2\%$, which is even lower than those examined by Tanaka et al. (1997), is so dilute as to be able to neglect the inter-particle collisions. The consideration of increase of drag coefficients in the vicinity of the wall was found to further increase the wall-normal RMS velocity fluctuations. It was also found that the wall-normal RMS velocity fluctuations increases as the increase of particle number density near the wall. Although the agreement between simulation and experiment was improved as compared to a simple one-way coupling simulation without drag increase near the wall, discrepancies were still significant. However, these results obviously suggest that the accordance between the LPT simulation and experimental data would possibly be improved by further accumulation of particles near the wall.

The main objective of the present paper is to study the influence of accumulation of particles near the wall on the structure of the dilute particulate turbulent flow near the wall and to understand the reason of discrepancies observed between simulations and experiments. For this purpose, different boundary conditions which will enhance the accumulation of particles near the wall are examined. The fluid flow is modeled using LES and the motion of particles are simulated by LPT. Two-way particle–fluid coupling, particle–particle collisions and wall–particle interactions are accounted for.

The paper is organized in the following way. In Section 2, the theoretical model is introduced. The studied cases and different boundary conditions used in those cases are described in Section 3. The computational procedure is outlined in Section 4. The results are presented and discussed in Section 5. Finally, in Section 6, the results are summarized and concluded.

2. Theoretical model

Similarly as the previous work introduced in the previous section, the turbulent channel flow was simulated using LES with a modified Smagorinsky subgrid scale (SGS) model (Zahrai et al., 1995), and the particles were tracked individually by integrating the particle equation of motion.

The governing equation for the LES, i.e., filtered continuity and Navier–Stokes equations, for an incompressible fluid with density, ρ^{f}, and kinematic viscosity, ν, can be expressed as

$$\frac{\partial \overline{u_i^{\mathrm{f}}}}{\partial x_i} = 0 \tag{1}$$

and

$$\frac{\partial \overline{u_i^{\mathrm{f}}}}{\partial t} = \frac{\partial}{\partial x_j}\left\{ -\overline{u_i^{\mathrm{f}} u_j^{\mathrm{f}}} - \frac{\overline{p}}{\rho^{\mathrm{f}}}\delta_{ij} + (\nu + \nu_{\mathrm{S}})\left(\frac{\partial \overline{u_i^{\mathrm{f}}}}{\partial x_j} + \frac{\partial \overline{u_j^{\mathrm{f}}}}{\partial x_i}\right)\right\} + \overline{\psi_i}, \tag{2}$$

where $\overline{u_i^{\mathrm{f}}}$ is the filtered fluid velocity, and $\overline{p}$ is the filtered pressure. The SGS viscosity, ν_{S}, was modeled by an anisotropic version of the Smagorinsky model. For details, the interested reader is referred to Zahrai et al. (1995). The last term, $\overline{\psi_i}$, represents the force from particles. Similarly as in the previous work (Fukagata et al., 1998a), $\overline{\psi_i}$ was modeled as a body force with the same magnitude, but in the opposite direction, as the averaged surface forces on particles, i.e.,

$$\overline{\psi_i} = -\frac{1}{\rho^{\mathrm{f}} V}\sum m\left(\frac{\mathrm{d}u_i^{\mathrm{p}}}{\mathrm{d}t} - g_i\right), \tag{3}$$

where V denotes the volume of the filter, i.e., the computational cell, and m is the particle mass. The summation in Eq. (3) is taken for all the particles in that cell. Influences of the presence of particles on the SGS model was neglected.

The particle equation of motion used in the present study can be written as

$$\frac{\mathrm{d}u_i^{\mathrm{p}}}{\mathrm{d}t} = C_i \frac{1}{\tau_{\mathrm{p}}}\left(1 + 0.15 Re_{\mathrm{p}}^{0.687}\right)\left(u_i^{\mathrm{f}} - u_i^{\mathrm{p}}\right) + g_i, \tag{4}$$

where u_i^{p} and u_i^{f} are the i-component of the particle velocity and the fictious fluid velocity at particle center, respectively. The first term of the particle equation of motion is the drag force and the second term is the gravitational force term. Effects of inter-particle collisions will be quantified in the numerical scheme in Section 4.

The Stokes relaxation time, τ_{p}, is defined as

$$\tau_{\mathrm{p}} = \frac{d^2 \rho^{\mathrm{p}}}{18 \nu \rho^{\mathrm{f}}}, \tag{5}$$

where d is the particle diameter and ρ^{p} is the particle density. The particle Reynolds number, Re_{p}, is defined by

$$Re_{\mathrm{p}} = \frac{|\vec{u}^{\mathrm{p}} - \vec{u}^{\mathrm{f}}|\, d}{\nu}. \tag{6}$$

The Reynolds number correction factor $(1 + 0.15 Re_{\mathrm{p}}^{0.687})$ in Eq. (4) was taken from the empirical formula by Schiller and Naumann (1933). This formula is, strictly speaking, valid for steady conditions only. However, effects due to particle acceleration were ignored similarly to the work by other researchers such as Wang and Squires (1996) and Tanaka et al. (1997).

The correction factor for the drag force term, C_i, represents the correction due to the presence of the wall. For the directions parallel to the wall, the expression by Faxén (1923),

$$C_1 = C_3 = \left[1 - \frac{9}{16}\left(\frac{d}{2y}\right) + \frac{1}{8}\left(\frac{d}{2y}\right)^3 - \frac{45}{256}\left(\frac{d}{2y}\right)^4 - \frac{1}{16}\left(\frac{d}{2y}\right)^5\right]^{-1}, \tag{7}$$

was used. For the direction normal to the wall, a model formula (Fukagata et al., 1999),

$$C_2 = \left[\left\{1 - \frac{9}{8}\left(\frac{d}{2y}\right) + \frac{1}{2}\left(\frac{d}{2y}\right)^3\right\}\left\{1 - \exp\left(-a\left(\frac{2y}{d} - b\right)\right)\right\}\right]^{-1}, \tag{8}$$

was applied. This model formula is based on the approximate solution by Wakiya (1960) and the exact solution, in a form of infinite series, by Brenner (1961). The constant, b, in the model formula is 1 in order to obtain similar exponential behavior near the wall as the solution by Brenner. Due to numerical reasons, it was set to $b = 0.9999$ in the simulations. The constant a was set to 2.686 (Fukagata et al., 1999).

The wall corrections on drag introduced above are based on the assumption of small, or possibly moderately small, values of Re_p. According to the experiment by Hallouin et al. (1998), the correction factor by Brenner (1961) significantly overestimates the drag coefficient for particles at $Re_p > 2.5$. Unfortunately, no expression is available at present for a drag correction factor near a wall at moderate Reynolds numbers and in a shear or in turbulence.

3. Problem description

The channel has a half width, δ, of 2 cm in y-direction and is assumed to be infinitely large in the streamwise, x, and the spanwise, z, directions. The dimensions of the computational domain is $\pi\delta \times 2\delta \times 0.5\pi\delta$ in x, y and z directions, as shown in Fig. 1, with periodic boundary conditions applied in x and z directions. Hereafter, for convenience in notation, x, y and z directions are sometimes also called as 1, 2 and 3 directions, especially when the direction appears as a subscript to variables.

For the fluid, air with a kinematic viscosity, ν, of 1.52×10^{-5} m^2/s was assumed. The wall-shear Reynolds number of the undisturbed fluid flow, Re_τ, defined by

$$Re_\tau = \frac{u_\tau \delta}{\nu}, \tag{9}$$

where u_τ is the shear velocity, was set to 644.

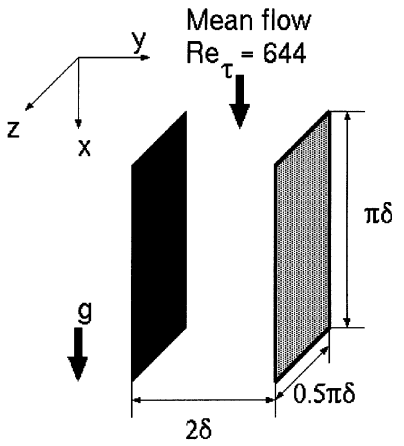

Fig. 1. Geometry of the channel.

For particles, copper particles with a diameter of 70 μm, corresponding to a value of $d^+ = 2.3$ in wall unit, were assumed. The corresponding Stokes relaxation time, τ_p^+, is 2000 wall unit. Gravitational force was set to $g_1^+ = 1.27 \times 10^{-3}$ and $g_2^+ = g_3^+ = 0$. These values correspond to the downward gravity of 9.8 m/s^2 in the physical space.

Five different cases, Cases 1–5, were examined according to different models for particle–wall impact in order to investigate the influence of accumulation of particles near the wall of each case as given in Table 1.

The particle–wall impact in Cases 1–3 is modeled as bounce with a restitution coefficient, r. If a particle impact the wall with velocity u_2^p, its velocity increment after impact is given by

$$\Delta u_2^p = -(1+r)\,u_2^p. \tag{10}$$

The streamwise and spanwise velocities, u_1^p and u_3^p, were assumed to be unchanged through the impact. The restitution coefficient, r was set to 1, 0.5 and 0 in Cases 1, 2 and 3, respectively.

For Cases 4 and 5, a model with a wall surface potential was used in order to further enhance the accumulation of particle near the wall. In this model, it is assumed that a particle with a diameter, d, and at a separation distance to a plane wall of $y_s = y - (d/2)$, experiences an attractive force, potential of which, Φ, can be approximated (see e.g. Friedlander, 1977) as

$$\Phi(y) = \frac{Ad}{12y_s}, \tag{11}$$

where A is known as Hamaker constant (Hamaker, 1937).

Using this wall potential, the following boundary conditions were introduced. When a particle hits the wall, the wall-normal component of the momentum is lost, similarly as in Case 3. In these cases, again, the streamwise and spanwise velocities were assumed to be unchanged through the impact. If the wall-normal velocity of the particle becomes greater than a critical velocity, V_c, due to re-acceleration by fluid dynamical forces or collisions with other particles, the particle is re-entrained with a velocity, $\sqrt{(u_2^p)^2 - V_c^2}$. Otherwise the particle stays at the wall. The critical velocity, V_c, which is the minimum velocity necessary for escaping from the wall potential, is given by

$$V_c = \sqrt{\frac{2\Phi(y_0)}{m}}, \tag{12}$$

where m is the mass of particle. The minimum separation length, y_0, was set at $y_0 = 4$ Å, which is similar to that used by Li and Ahmadi (1993) who studied the deposition problem in a turbulent particulate flow.

Table 1
The restitution coefficient, r, Hamaker constant, A, the number of particles used in the simulation, N_0, and computed mass flow ratio, Z, for each case

	r	A ($\times 10^{-20}$ J)	N_0	Z (%)
Case 1	1	0	1500	1.99
Case 2	0.5	0	1600	2.04
Case 3	0	0	1800	1.95
Case 4	0	18	1900	1.98
Case 5	0	180	2500	1.97

The Hamaker constant between a copper particle and a glass wall, materials used in the experiment by Kulick et al., can be computed as $A = 18.0 \times 10^{-20}$ J using the Hamaker constants of copper and glass (Dahneke, 1972), $A_{\mathrm{copper}} = 28.3 \times 10^{-20}$ J and $A_{\mathrm{glass}} = 11.5 \times 10^{-20}$ J, in the relation by Boehme et al. (1969),

$$A = \sqrt{A_{\mathrm{copper}} A_{\mathrm{glass}}}. \tag{13}$$

In Case 4, the Hamaker constant calculated above, $A = 18.0 \times 10^{-20}$ J, was used. In Case 5, a value of 10 times larger than that in Case 4, $A = 180 \times 10^{-20}$ J, was used in order to see the effect of wall potential more clearly.

4. Computational procedure

The number of cells used in LES are $32 \times 42 \times 96$ in x, y and z directions. The mesh is stretched in y direction so that the cells are finer near the wall and coarser in the center of the channel. The corresponding mesh spacing in each direction is shown in Table 2. The superscript, $+$, denotes the variables in wall unit.

At the beginning of the simulation, the particles were homogeneously distributed in the whole channel where a fully developed velocity field for fluid had already been computed. The initial particle velocities were set to the local fluid velocities. For the computation of the particle equation of motion, Eq. (4), a fourth-order Lagrangian interpolation was used for obtaining the fluid velocity at the particle locations. Both the filtered Navier–Stokes equation and the particle equation of motion were integrated using a third-order Adams–Bashforth scheme with a time step of $\Delta t^+ = 0.322$. The statistics were accumulated for about 4000 wall time units after that the flow had been fully developed, typically after about 10 000 wall time units from the initial state. The convergence of the flow statistics was assured by monitoring the global balance of momentum and energy of particles, similarly as in Fukagata et al. (1998b).

The number of particles used in the simulations varied for different cases, as shown in Table 1, in order to keep the mass flow ratio, Z, defined by

$$Z = \frac{\sum m^{\mathrm{p}} u^{\mathrm{p}}}{\int \rho^{\mathrm{f}} u^{\mathrm{f}} \, \mathrm{d}V}, \tag{14}$$

where m^{p} is the mass of a particle, constant. Results show that $Z = 2 \pm 0.05\%$ in the fully developed flow for all cases despite all changes in the structure of the flow due to the changes in particle boundary conditions, as shown in Table 1.

The computational procedure for the inter-particle collisions used in the present study is as the following. At first, provisional positions of the particles at time $(t + \Delta t)$ are computed without taking into account collisions, as represented by dotted circles in Fig. 2. For the judgement

Table 2
Mesh specifications

N_x	N_y	N_z	Δx^+	$\Delta y^+_{\mathrm{min}}$	$\Delta y^+_{\mathrm{max}}$	Δz^+
32	42	96	63.2	2.9	109.7	10.5

whether collisions occur between two neighboring particles, the method described by Yamamoto et al. (1998) can be used. Namely, two particles, labeled as Particles 1 and 2 as shown in Fig. 2, can be judged to collide if the equation about the distance between their trajectories,

$$\left|\vec{x}^{\mathrm{R}}(t) + k(\vec{x}^{\mathrm{R}*}(t+\Delta t) - \vec{x}^{\mathrm{R}}(t))\right|^2 = d^2, \tag{15}$$

has two real roots, k_1 and k_2 ($k_1 \leqslant k_2$), and the value of smaller real root, k_1, is between 0 and 1, i.e., $0 \leqslant k_1 \leqslant 1$. Here, $\vec{x}^{\mathrm{R}}(t)$ is the position of Particle 1 relative to Particle 2 at time t, i.e.,

$$x_i^{\mathrm{R}}(t) = x_i^{(1)}(t) - x_i^{(2)}(t), \tag{16}$$

and $\vec{x}^{\mathrm{R}*}(t+\Delta t)$ is the provisional position of Particle 1 relative to Particle 2 at time $(t+\Delta t)$. If these particles are judged to collide, the normal unit vector from the center of Particle 2 to the center of Particle 1 at the contact, $\vec{n}^{\mathrm{R}}$, can be computed as

$$n_i^{\mathrm{R}} = \frac{1}{d}\left\{x_i^{\mathrm{R}}(t) + k_1(x_i^{\mathrm{R}*}(t+\Delta t) - x_i^{\mathrm{R}}(t))\right\}. \tag{17}$$

By assuming here a perfectly elastic collision, the velocity increment of Particles 1 and 2 due to the collision, $\Delta u_i^{(1)}$ and $\Delta u_i^{(2)}$, can be computed by

$$\Delta u_i^{\mathrm{p}(1)} = -u_j^{\mathrm{R}}(t)\, n_j^{\mathrm{R}} n_i^{\mathrm{R}}, \quad \Delta u_i^{\mathrm{p}(2)} = +u_j^{\mathrm{R}}(t)\, n_j^{\mathrm{R}} n_i^{\mathrm{R}}, \tag{18}$$

where $u_i^{\mathrm{R}}(t)$ is the relative velocity before collision,

$$u_i^{\mathrm{R}}(t) = u_i^{(1)}(t) - u_i^{(2)}(t). \tag{19}$$

A perfectly elastic collision was assumed in the present study. For more general expression including an inelastic collision, particle rotation and friction between colliding particles, reader is referred to Yamamoto et al. (1998).

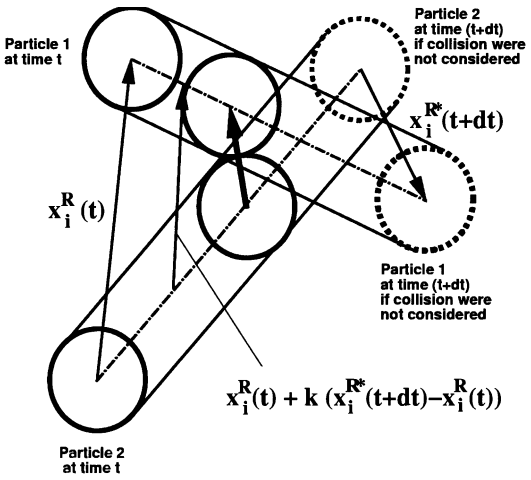

Fig. 2. Computation of a inter-particle collision.

5. Results

In this section, reported are results from simulations of particulate turbulent channel flow where inter-particle collisions are accounted for. The focus of the description is placed on the investigation of effects of particle wall boundary conditions on statistical behavior of the flow.

Figs. 3 and 4 show the mean velocity and the RMS levels of velocity fluctuations of the fluid in a flow without any particles. Although the mesh spacing in y direction in the center of channel, $\Delta y^+_{\max} = 109.7$, is likely to be coarse for a large eddy simulation, comparison of these statistics with experimental data of Kulick et al. (1994) indicated that the fluid velocity field was computed with a reasonable accuracy.

It was found that the statistics of the fluid were not different from those in unladen flow for all the cases studied here. The observation that the statistics of fluid is unaffected by presence of 70 μm copper particles for the case of $Z = 2\%$ is in accordance with the experimental observation by Kulick et al. (1994), except for the wall-normal velocity fluctuations of which a slight reduction of RMS value in bulk of the channel as compared to that in the unladen flow was observed in the experiment.

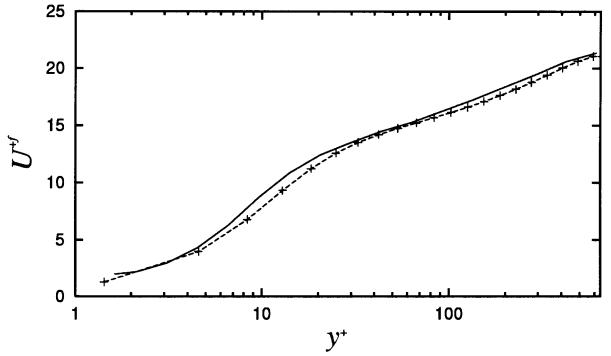

Fig. 3. Mean velocity of the undisturbed flow at $Re_\tau = 644$. $- + -$, LES in this study; ———, experiment by Kulick et al. (1994).

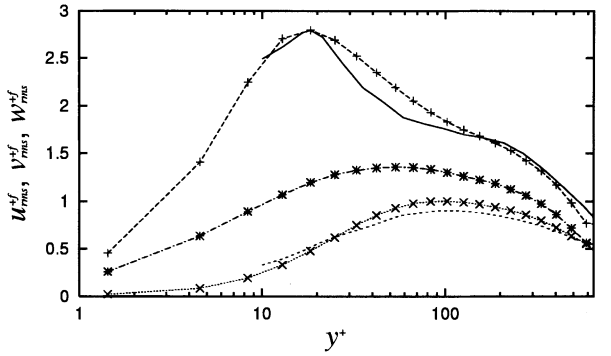

Fig. 4. RMS levels of the undisturbed flow at $Re_\tau = 644$. $- + -$, $u^{+\mathrm{f}}_{\mathrm{rms}}$; - - × - -, $v^{+\mathrm{f}}_{\mathrm{rms}}$; ⋯ ∗ ⋯, $w^{+\mathrm{f}}_{\mathrm{rms}}$; LES in this study. ———, $u^{+\mathrm{f}}_{\mathrm{rms}}$; - - - - -, $v^{+\mathrm{f}}_{\mathrm{rms}}$; experiment by Kulick et al. (1994).

Fig. 5(a)–(c) show the mean and RMS values of particle velocities. Only Cases 1, 3 and 5 are presented, because no significant differences could be observed between Cases 1 and 2, and between Cases 3 and 4. The mean particle velocity , $U^{+\mathrm{p}}$, in Case 5 is in a good agreement with the experimental data, except for the near-wall region, $y^+ < 10$. The values of $U^{+\mathrm{p}}$ are slightly over-predicted in Case 1 and under-predicted in Case 3 in whole channel. An abrupt increase of $U^{+\mathrm{p}}$ in $y^+ < 10$ region in the experimental data was not reproduced in any case of the present simulations.

In all cases, the profile of $U^{+\mathrm{p}}$ show better agreement with the experimental data in the present simulations than that of the one-way coupling simulation by Wang and Squires (1996). One may consider that this improvement of the simulation data in the present study over those in Wang and Squires is caused by the introduction of extra effects, i.e., inter-particle collisions and drag cor-

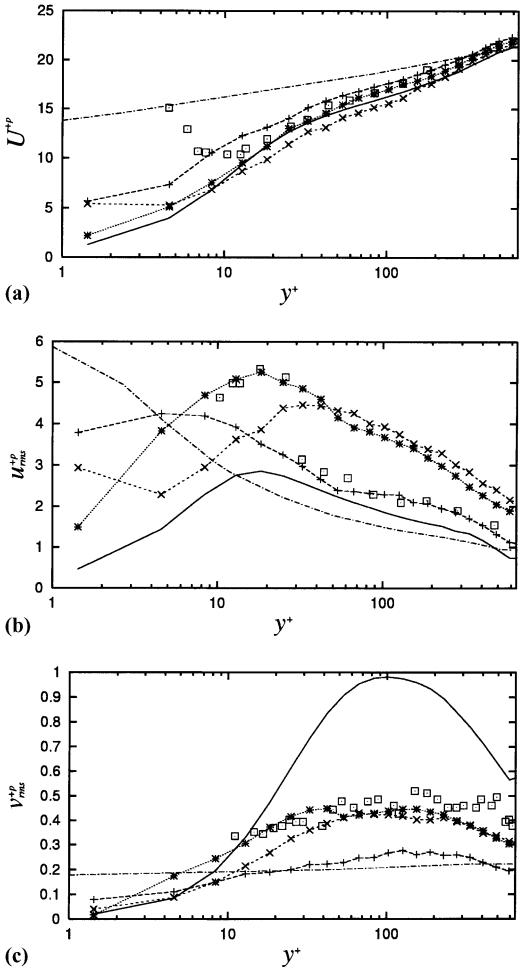

Fig. 5. Particle statistics: (a) mean velocity; (b) RMS streamwise velocity; (c) RMS wall-normal velocity. $-+-$, Case 1; - - × - -, Case 3; - - ∗ - -, Case 5. —- —, one-way coupling LES by Wang and Squires (1996); □, experiment by Kulick et al. (1994), $Z = 2\%$; (———, undisturbed fluid.)

rection near the wall, in the present study. However, it was observed in the previous study (Fukagata et al., 1999) that the differences in mean particle velocities computed using four-way coupling and one-way coupling simulations were not significant, and that the increase of drag coefficient near the wall had only a little effect on the mean velocity. Furthermore, the discrepancy observed here is similar to that appears when the flow of particles is not fully developed, see Fukagata et al. (1998b). Therefore, we can conclude that the discrepancy in the mean velocity is more likely due to an insufficient development time used in the simulation by Wang and Squires (1996).

The RMS level of streamwise particle velocity, $u^{+\mathrm{p}}_{\mathrm{rms}}$, in Case 1 shows similar values as those of the experimental data in $y^+ > 30$ region. The profile in Case 3 and that in Case 5 are similar and have a local maximum value as in the case of the experimental data. The peak of the profile in Case 5 almost coincides with the experimental data. However, Cases 3 and 5 predicted significantly higher values in the outer region, $y^+ > 30$ than those from experiments.

The RMS level of wall-normal velocity, $v^{+\mathrm{p}}_{\mathrm{rms}}$, in Case 1 is almost half of that in the experiment, while in Cases 3 and 5 it shows a good agreement with the experimental data.

The probability distribution function (PDF) of the streamwise particle velocity around $y^+ = 12$ plane is shown in Fig. 6. A clear bimodal distribution similar to the experimental data is only observed in Case 5. The profile for Case 3 also shows a weak bimodality. Assuming that these two modes can be separated at $u^{+\mathrm{p}} = 12$, the mean value of lower mode, $U^{+\mathrm{p}}_{\mathrm{L}}$,

$$U^{+\mathrm{p}}_{\mathrm{L}} = \frac{1}{P_{\mathrm{L}}} \int_{-\infty}^{12} u^{+\mathrm{p}} P(u^{+\mathrm{p}})\, \mathrm{d}u^{+\mathrm{p}}, \tag{20}$$

the mean value of higher mode, $U^{+\mathrm{p}}_{\mathrm{H}}$,

$$U^{+\mathrm{p}}_{\mathrm{H}} = \frac{1}{P_{\mathrm{H}}} \int_{12}^{+\infty} u^{+\mathrm{p}} P(u^{+\mathrm{p}})\, \mathrm{d}u^{+\mathrm{p}}, \tag{21}$$

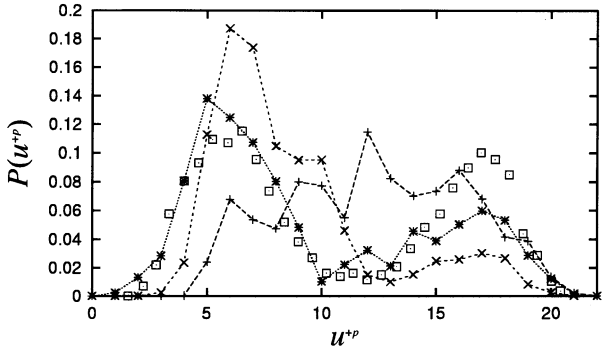

Fig. 6. PDF of streamwise particle velocity at $y^+ = 12$ plane. $-+-$, Case 1; - - × - -, Case 3; - - ∗ - -, Case 5; □, experiment by Kulick et al. (1994), $Z = 2\%$.

and the probability of each mode, P_L and P_H,

$$P_L = \int_{-\infty}^{12} P(u^{+p})\, du^{+p} \tag{22}$$

and

$$P_H = \int_{12}^{+\infty} P(u^{+p})\, du^{+p}, \tag{23}$$

can be calculated using the data in Fig. 6, as shown in Table 3. It was found that the mean values and the probabilities of modes calculated from the simulation data became closer to the values of the experimental data as the wall potential was increased.

The global behavior of the PDF for all y^+ positions in half of the channel is presented in Fig. 7. The values of $P(u^{+p})$ are normalized such that the integral over u^{+p}, at a fixed y^+, is unity. According to Fig. 7, bimodality is not observed at any position in the channel in Case 1, while it is pronounced in the region of $20 < y^+ < 50$ in Case 3 and $12 < y^+ < 25$ in Case 5. In the near-wall region, $y^+ < 10$, high velocity particles coming toward the wall are decelerated basically by low velocity fluid in Case 1. In Cases 3 and 5, however, the velocity of particles seems to drop faster and no or few particles with high velocities can be observed near the wall. In the bulk region, $y^+ > 40$, high velocity particles are present in all cases, while the existence of low velocity particles which cause high values of u_{rms}^{+p} is evident only in Cases 3 and 5.

It can be concluded from these observations on PDF that the profiles of U^{+p} and u_{rms}^{+p} in the region where bimodality exists will largely depend on the ratio between the total number of particles in the higher mode and that in the lower mode. Although the mean value of each mode at $y^+ = 12$ in Case 3 seems to be similar to that in the experiment, the values of U^{+p} and u_{rms}^{+p} at $y^+ = 12$ became different from the experiment due to the difference in the ratio between higher and lower modes, P_H/P_L. In Case 5, the values of U^{+p} and u_{rms}^{+p} are closer to the experimental data because P_H/P_L becomes closer to the experimental value.

The cause of the occurrence of this bimodality in Cases 3 and 5 can also be investigated by studying a snapshot of correlations of (u^{+p}, v^{+p}) taken in the region $10 < y^+ < 20$, which is shown in Fig. 8. Different groups of particles can be identified here. The first group consists of particles with high values of u^{+p} and negative values of v^{+p}. These particles are those coming from the center of the channel and moving toward the wall. The second group consists of the particles with intermediate velocity and almost zero wall-normal velocity. In Case 1, another family of high velocity particles can be identified, this time with a positive value of v^{+p}, which corresponds to particles leaving the near-wall region after an impact at the wall. In Cases 3 and 5, this last group of particles moving away from the wall, have a low streamwise velocity, typically less than six, i.e., high velocity particles moving away from the wall are missing.

Table 3
Mean velocities and probabilities of lower and higher modes

	U_L^{+p}	U_H^{+p}	P_L	P_H	P_H/P_L
Case 3	7.21	15.29	0.82	0.18	0.22
Case 4	6.75	15.33	0.79	0.21	0.27
Case 5	6.08	15.82	0.65	0.35	0.54
Experimental data	6.26	16.52	0.57	0.43	0.75

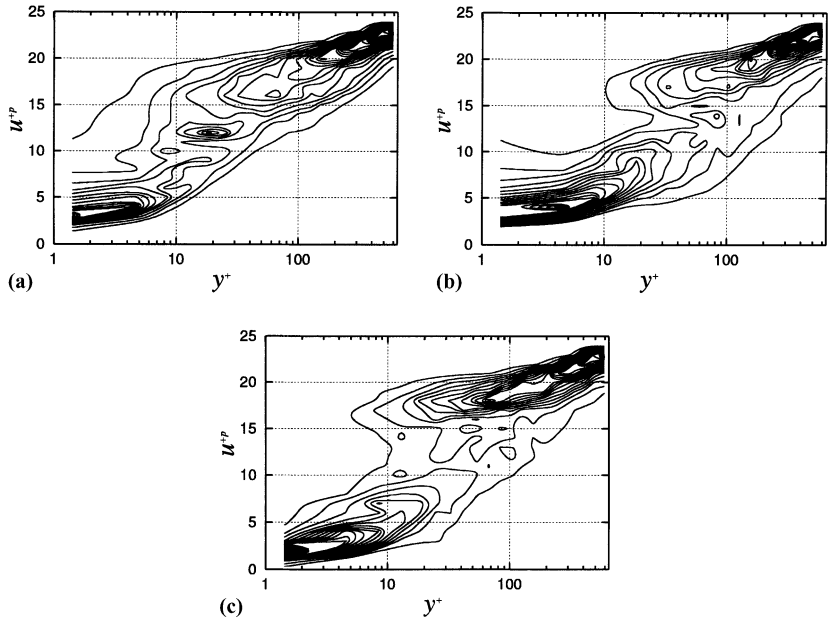

Fig. 7. PDF contour of streamwise particle velocity: (a) Case 1; (b) Case 3; (c) Case 5. Difference between level lines is 0.02.

From the results presented above, it can be concluded that the suppression of the entrainment process reduces the maximum value of the lower mode while a reduced number of particles with low streamwise velocity results in an increase of the maximum value of the higher mode. The statistical behavior in Case 3 and that in Case 5 was found to be qualitatively the same. The quantitative difference between these was only due to the different rate of entrainment from the near-wall region. Therefore in the following discussions about inter-particle collisions, comparisons are made only between Cases 1 and 3. The same discussions are valid between Cases 1 and 5.

Fig. 9 shows the number of particles in a wall unit volume, N^+, and the collision frequency, f_c^+, defined as the number of collisions in a wall unit volume per a wall unit time. In both Cases 1 and 3, collisions in the vicinity of the wall occurs far more frequently than in the bulk flow. The particle number density at the sample point nearest to the wall in Case 3 is about 10 times larger than that in Case 1 and the collision frequency is about 100 times larger. In the bulk region, the collision frequencies and number density have similar values in Cases 1 and 3.

Fig. 10 shows the mean change of streamwise velocity of particles, here labeled as Particle 1, due to collisions. The label was defined such that Particle 1, one of the colliding pair, has always a larger approaching velocity toward the wall than the other one, Particle 2. In both cases, the streamwise velocity of these particles in average decreased after the collisions. The tendency is most clear in the buffer region, say $20 < y^+ < 60$, in Case 3. This phenomena can be explained by a scenario consisting of the following steps: (1) a particle which has obtained high streamwise velocity in the center of the channel approaches toward the wall; (2) the particle collides with a particle in the cloud of low velocity particles existing in the buffer regions and (3) the particle

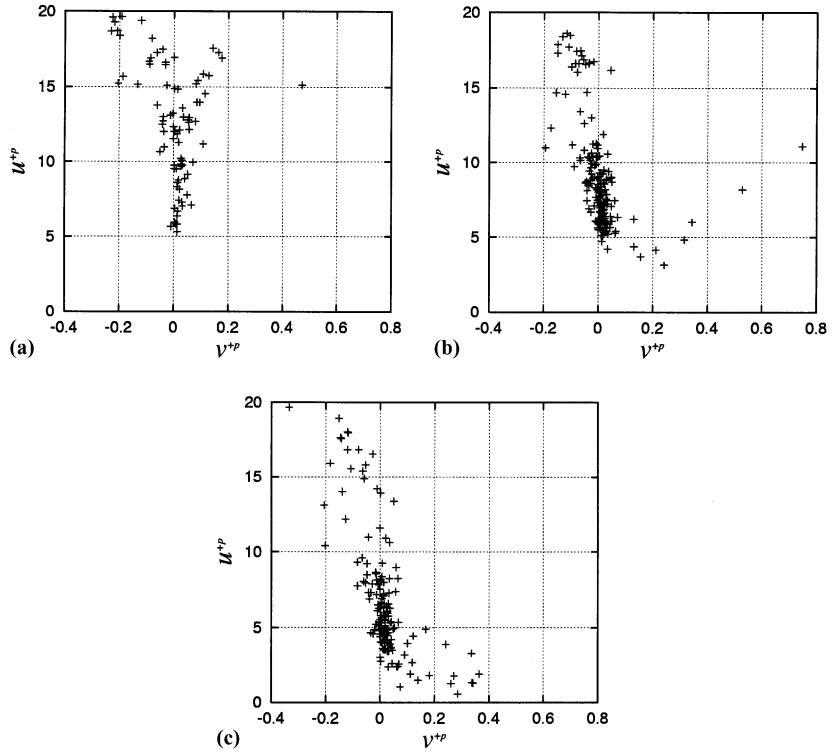

Fig. 8. Phase space distribution of particle velocity at $y^+ = 12$: (a) Case 1; (b) Case 3; (c) Case 5.

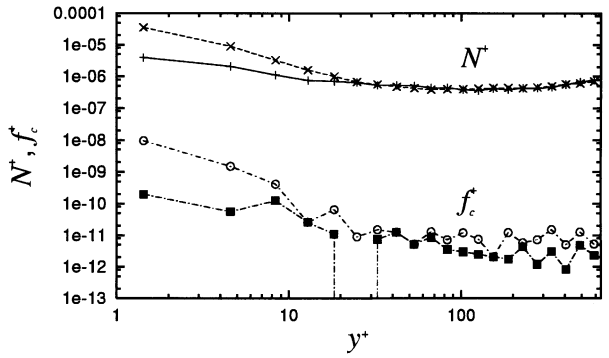

Fig. 9. Particle number density, N^+, and collision frequency, f_c^+. $-+-$, N^+ for Case 1; - - × - -, N^+ for Case 3; $\cdots\blacksquare\cdots$, f_c^+ for Case 1; - · ⊖ · -, f_c^+ for Case 3.

largely loses its streamwise momentum. Such drop of streamwise velocity is also contributing to the decrease of PDF of higher velocity mode in the buffer region.

The correlations between different components of velocity of Particle 1 relative to Particle 2, $u^{+\mathrm{R}}$ and $v^{+\mathrm{R}}$, before and after collisions, are plotted in Fig. 11. In Case 3, the distribution is highly

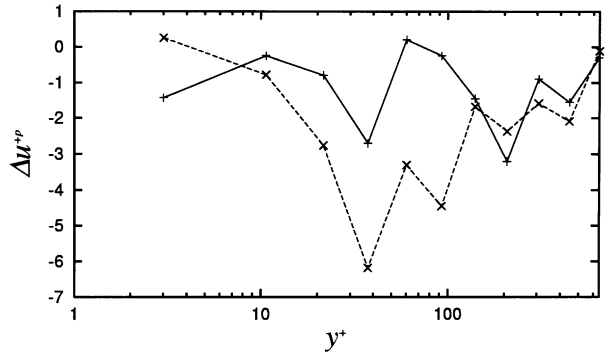

Fig. 10. Streamwise velocity change at collision of particle approaching to the wall. – – + – –, Case 1; - - × - -, Case 3.

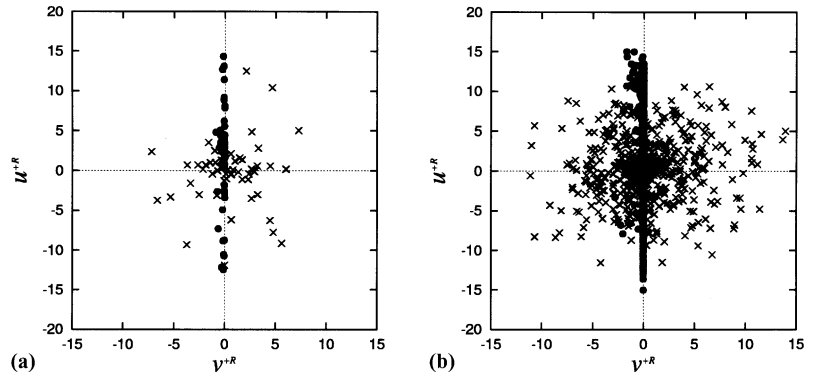

Fig. 11. Correlation between u^{+R} and v^{+R}: (a) Case 1; (b) Case 3. ●, before collisions; ×, after collisions.

anisotropic before collisions and is isotropic after the collisions. This means that the streamwise component of the velocity is partly converted to wall-normal velocity component due to collisions. Although the number of sample points is few in Case 1, a similar behavior is observed.

The high RMS wall-normal velocity observed in Case 3 can be related to more frequent collisions in the near-wall region than those in Case 1. Due to large relaxation time of particles, such high wall-normal velocities in the near-wall region also result in high v^{+p}_{rms} in the bulk of the flow. Values of v^{+p}_{rms} become even higher in the bulk flow, as shown in Fig. 5(c), because the relative importance of the particles with high wall-normal velocity increases as the total number of particles decreases.

Making use of all the information above, the presence of bimodal probability distribution function can be explained as follows. With purely elastic collisions between particles with long relaxation time and the wall, particles entering the near-wall region leave it after an impact, and thereby a reflection appears at the wall. The particle loses part of its energy only due to viscous effects. How large it will be depends on the relaxation time of the particle and the direction of its motion relative to the wall. In such case, particles of different streamwise velocities would be present in the near-wall region with a mono-modal probability distribution function.

On the other hand, if there is any mechanism that can prevent all or parts of particles to move freely away from the wall, a cloud of low velocity particles will be formed in the vicinity of the wall. Parts of these particles will be injected into the flow. A particle which enters the near-wall region meets the low velocity cloud of particles and loses its directional velocity due to particle–particle collisions in an efficient way. This creates a group of particles with a probability distribution function strongly dependent on the conditions at the wall.

For the latter case of flow, with certain combination of parameters, the two family of particles, i.e., the one with low streamwise velocity created near the wall and the one with high streamwise velocity coming from the outer region, can co-exist at a certain distance to the wall. If their mean directional velocity is sufficiently different, a bimodal probability distribution function will be observed.

It should be mentioned that the above explanation of the cause of bimodality of the probability distribution function is a detailed version of that given by Kulick et al. (1994) with a slight modification. Here, it is claimed and shown that an additional mechanism than hydrodynamical effects is needed to trap the particle near the wall to create bimodal probability distribution function.

Finally, the creation of the low velocity cloud of particles near the wall and an efficient scattering of high velocity particles give a clear contribution to non-directional velocities which can be observed in the whole channel. As a result, sufficiently higher RMS levels in the wall-normal component of the particle velocity, in good agreement with experimental data, were predicted when an attractive force was present near the wall.

As mentioned in Section 2, the formula used for near-wall drag correction is valid for low particle Reynolds numbers only. Use of that formula might have overestimated the drag force since the simulation data show, see e.g. Fig. 7(b), that the probability density of particles with high Reynolds numbers, say around 10, i.e., $u^{+\mathrm{p}} \simeq 4$, in the near-wall region is not negligible. In order to ensure the discussions made above, Case 3 was re-computed without the near-wall drag correction. Figs. 12 and 13 show the RMS wall-normal particle velocity and PDF of streamwise particle velocity in Case 3 with and without near-wall drag correction. However, the RMS levels of wall-normal particle velocity and the PDF of streamwise particle velocity seem not to be sensitive to the choice of formula of near-wall drag correction.

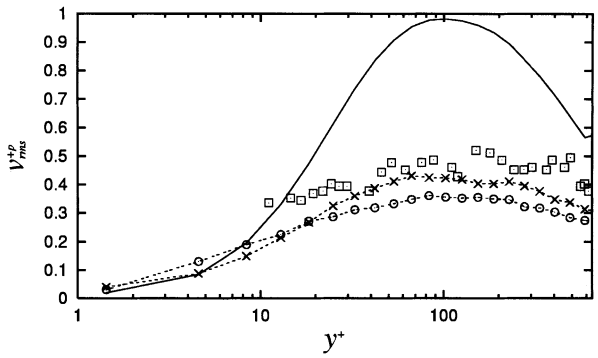

Fig. 12. RMS levels of wall-normal particle velocity of Case 3 with and without near-wall drag correction. - - × - -, with correction; - - ○ - -, without correction. □, experiment by Kulick et al. (1994), $Z = 2\%$; (———, undisturbed fluid.)

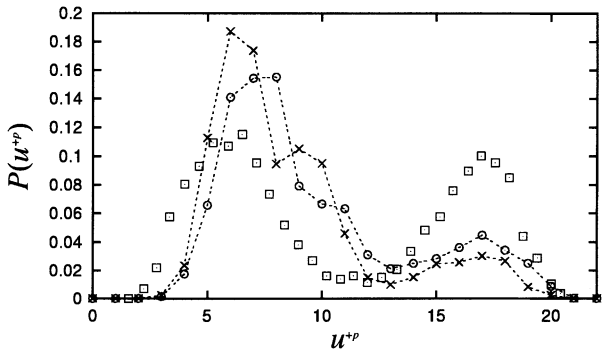

Fig. 13. PDF of streamwise particle velocity of Case 3 with and without near-wall drag correction. - - × - -, with correction; - - ○ - -, without correction. □, experiment by Kulick et al. (1994), $Z = 2\%$.

6. Conclusions

Analyses were made to clarify the general discrepancy found between results from numerical simulations and data from physical experiments of dilute particulate channel flow. The flow of 70 μm copper particles in a turbulent channel at low mass loading of 2% investigated by Kulick et al. (1994) was chosen as a reference case. Fluid flow was modeled using LES. Motion of particles was followed by LPT taking into account binary particle–particle collisions. The influence of wall–particle interaction on the statistical behavior of the flow was investigated by using different particle boundary conditions at walls.

The present analyses showed that the impact model for particles near the wall, or in a more general term, the model used for the particle–wall interaction has a very strong effect on the structure of the flow in the whole channel. This observation can be attributed to the fact that in a dilute flow of particles with long relaxation time, the history that each particle experiences has a direct influence on all the statistics. Secondly, particle–particle collisions are unexpectedly of crucial importance even at low mass loading. The reasons for this could be clearly illustrated.

In the present study, the bimodality of the probability distribution function that was observed in experimental investigations but not in the past numerical simulations, could be observed clearly. It was shown that this bimodality is caused by a mechanism that could suppress a direct re-entrainment of particles after an impact at the wall. Such an effect will increase the number density of particles in the vicinity of the wall and creates a source of low velocity particles to be injected into the flow.

The low velocity particles in the near-wall region interacts with high velocity particles coming from the bulk of the flow and results in scattering of those particles. This scattering near the wall increases the RMS levels of the wall-normal component of the particle velocity in the whole channel.

The bimodality of the probability function and the increase of RMS levels of the wall-normal components mentioned above were enhanced when the particles were trapped in a potential near the wall. The use of such potential changes the probability distribution function of particles near the wall, increases the number density near the wall and contributes to scattering of high velocity particles entering the near-wall region.

The lack of bimodality of the probability distribution function and sufficiently lower RMS levels in the wall-normal component of the particle velocity in previous simulations of the case studied here are therefore attributed to the use of purely elastic collisions at the wall and the neglect of inter-particle collisions.

Although the present simulations could reproduce the anomalous behavior of velocity fluctuations similar to those observed in the physical experiment, the cause of the phenomena can be different. As examples, small electrostatic charges and surface roughness may have similar amplifying effects on the statistics of particle flows. According to the present results, wall–particle interaction must be treated with special care in both experimental and numerical investigations of dilute flow of heavy particles. The situation is certainly different for flows at high particle number density and particles with short relaxation time, but not likely to be less complex.

References

Boehme, G., Krupp, H., Schnabel, W., 1969. In: Dranflis, et al. (Eds.), Molecular Processs on Solid Surfaces. McGraw-Hill, New York.

Brenner, H., 1961. The slow motion of a sphere through a viscous fluid towards a plane surface. Chem. Eng. Sci. 16, 242–251.

Dahneke, B., 1972. The influence of flattening on the adhesion of particles. J. Colloid Interface Sci. 40, 1.

Faxén, H., 1923. Die Bewegung einer starren Kugel Längs der Achse eines mit zaher Flüsigkeit fefüllten Rohres. Arkiv för Matematik, Astronomi och Fysik 17 (27), 1–28.

Friedlander, S.K., 1977. Smoke, Dust and Haze. Wiley, NewYork, p. 45.

Fukagata, K., Zahrai, S., Bark, F.H., 1998a. Fluid stress balance in a turbulent particulate channel flow. In: Proceedings of the Third International Conference on Multiphase Flow (CD-ROM), Paper 157, pp. 1–8.

Fukagata, K., Zahrai, S., Bark, F.H., 1998b. Force balance in a turbulent particulate channel flow. Int. J. Multiphase Flow 24, 867–887.

Fukagata, K., Zahrai, S., Bark, F.H., Kondo S., 1999. Influences of the near-wall drag correction in a Lagrangian simulation of particulate turbulent channel flow. In: Proceedings of the First Symposium on Turbulence and Shear Flow Phenomena. Begell House, Santa Barbara, 12–15 Septemper 1999, pp. 259–264.

Gore, R.A., Crowe, C.T., 1989. Effect of particle size on modulating turbulent intensity. Int. J. Multiphase Flow 15, 279–285.

Hallouin, E., Gondret, P., Lance, M., Petit L., 1998. On the motion of a sphere toward a plane surface: from lubrication to bouncing regime. In: Proceedings of the Third International Conference on Multiphase Flow (CD-ROM), Paper 703, pp. 1–9.

Hamaker, H.C., 1937. The London-van der Waals' attraction between spheroid particles. Physica 4, 1058.

Hetsroni, G., 1989. Particles-turbulence interaction. Int. J. Multiphase Flow 15, 735–746.

Hetsroni, G., Sokolov, M., 1971. Distribution of mass, velocity, and intensity of turbulence in a two-phase turbulent jet. J. Appl. Mech. 38, 315–327.

Kulick, J.D., Fessler, J.R., Eaton, J.K., 1994. Particle response and turbulence modification in fully developed channel flow. J. Fluid Mech. 277, 109–134.

Li, A., Ahmadi, G., 1993. Deposition of aerosols on surfaces in a turbulent channel flow. Int. J. Eng. Sci. 31, 435–451.

Maeda, M., Hishida, K., Furutani, T., 1980. Optical measurement of local gas and particle velocity in an upward flowing dilute gas–solids suspension. Polyphase Flow and Transport Technology. Century 2-ETC, San Francisco, CA, pp. 211–216.

Rouson, D.W.I., Eaton, J.K., 1994. Direct numerical simulation of particles interacting with a turbulent channel flow. In: Proceedings of the Seventh Workshop on Two-phase Flow Predictions. Erlangen, Germany.

Schiller, L., Naumann, A., 1933. Über die grundlegenden Berechungen bei der Schwerkraftaufbereitung. Vereines Deutscher Ingenieure 77, 318.

Tanaka, T., Yamamoto, Y., Potthoff, M., Tsuji, Y., 1997. LES of gas-particle turbulent channel flow. In: Proceedings of 1997 ASME Fluid Engineering Division Summer Meeting (CD-ROM), FEDSM97-3630, pp. 1–5.

Wakiya, S.J., 1960. Research Report 9. Faculty of Engineering, Niigata University, Japan.

Wang, Q., Squires, K.D., 1996. Large eddy simulation of particle-laden turbulent channel flow. Phys. Fluids 8, 1207–1223.

Yamamoto, Y., Tanaka, T., Tsuji, Y., 1998. LES of gas-particle turbulent channel flow (The effect of inter-particle collision on structure of particle distribution). In: Proceedings of the Third International Conference on Multiphase Flow (CD-ROM), Paper 518, pp. 1–7.

Zahrai, S., Bark, F.H., Karlsson, R.I., 1995. On anisotropic subgrid modeling. Eur. J. Mech. B 14, 459–486.

Zisselmar, R., Molerus, O., 1979. Investigation of solid–liquid pipe flow with regard to turbulence modification. Chem. Eng. J. 18, 233–239.